Miniature Resonant Ambulatory Robot

Shannon A. Rios, Andrew J. Fleming, and Yuen Kuan Yong

***Abstract*—This article describes the design, manufacture, and performance of a prototype miniature resonant ambulatory robot that uses piezoelectric actuators to achieve locomotion. Each leg is comprised of two piezoelectric bimorph benders, joined at the tip by a flexure and end effector. Combinations of amplitude and phase can be used to produce a wide range of motions including swinging and lifting. A lumped mass model previously developed is described as a design tool to tune the resonance modes of the end effector. The completed robot was driven with frequencies up to 500 Hz resulting in a maximum forward velocity of approximately 520 mm/s at 350 Hz. A frequency analysis was also performed to determine the effects of ground contact on the performance of the robot. This analysis showed a significant reduction in the resonance gain and frequency.**

***Index Terms*—Multilegged robots, mechanism design of mobile robots.**

I. Introduction

THERE are many advantages to the miniaturization of autonomous robots. Their reduction in size allows the robot access to restricted locations, for example inside water pipes [1], through rubble [2]–[4], and even inside the human body [5]. The smaller size also creates a potential for cost reduction and the capability of disposable robots [6]. Additionally, due to the small power requirements, it may be possible to power a miniature robot from ambient energy sources such as light, electric fields, magnetic fields, or vibration [7], [8]. Despite these advantages, there are several challenges present when designing miniature robots. As the size of the robot decreases, it becomes more difficult to implement a complex mechanical and electrical design and the available footprint for sensors, actuators and computational power is reduced.

Over the past decade, there has been an increased interest in the development of miniature robots [9]. For example, Wood *et al.* have developed several miniature robots utilizing piezoelectric bender actuators for locomotion [10]–[14]. One such example is a 1.7 g hexapod robot that was able to achieve a forward travel speed of 0.9 body lengths per second [15]. This robot was approximately 4.8 cm long and consisted of three leg pairs where each pair of legs were driven by three piezoelectric benders arranged to amplify the displacement and produce a tripod gait.

Manuscript received April 12, 2016; revised August 6, 2016; accepted September 25, 2016. Date of publication October 3, 2016; date of current version October 17, 2016. This paper was recommended for publication by Associate Editor N. Tsagarakis and Editor A. Bicchi upon evaluation of the reviewers' comments.

The authors are with the Precision Mechatronics Laboratory, School of Electrical Engineering and Computer Science, University of Newcastle, Callaghan, NSW 2308, Australia (e-mail: Shannon.Rios@newcastle.edu.au; Andrew.Fleming@newcastle.edu.au; Yuenkuan.Yong@newcastle.edu.au).

Color versions of one or more of the figures in this letter are available online at http://ieeexplore.ieee.org.

Digital Object Identifier 10.1109/LRA.2016.2614837

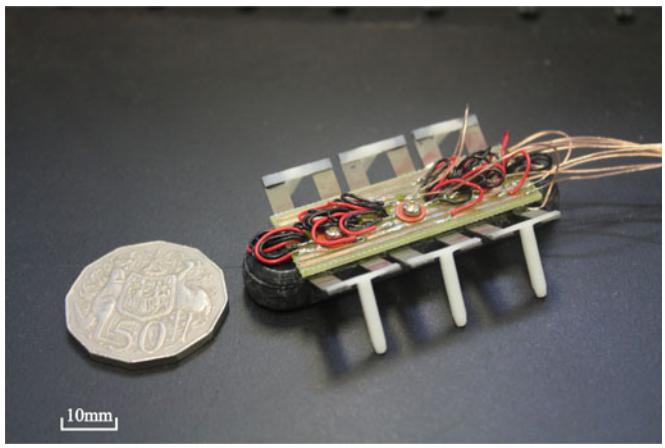

Fig. 1. MinRAR V1 prototype robot.

Nguyen *et al.* have produced a meso-scaled hexapod robot driven by 'soft' dielectric elastomer actuators [16]. The constructed robot weighed approximately 80 g and was able to achieve a forward locomotion speed of 4 mm/s when driven with a 3.5 kV square wave at 0.5 Hz.

Another example of a miniature piezoelectric robot is highlighted in the works of Oldham *et al.* This work focused on the modeling, control and manufacture of multi-degree-of-freedom microrobotic legs that utilize thin-film PZT actuators [17], [18]. It is estimated that a robot using this form of actuator would achieve a forward locomotion speed of 27 mm/s. Additional work has characterized the effect of dynamic contact iterations on micro-robotic leg structures [19].

An example of a novel approach to miniature robotic locomotion can be seen in the works of Hariri *et al.* [20]–[22]. These works outline the design and development of a meso-scaled robot driven by a traveling wave in an aluminum beam. The traveling wave is excited by one or two piezoelectric patches at either end of an aluminum beam and the speed of the robot can be controlled by varying the amplitude of the voltage. Another robot developed by Hariri *et al.* uses a similar method to excite a standing wave on a legged robot [23]. These robots are able to achieve a forward locomotion speed of 246.5 mm/s and 40 mm/s respectively.

The use of resonant vibration in miniature robotics was also reported by Becker *et al.* in their work on piezo-driven micro robots [24]. Their work outlines the development of a range of robots capable of traveling over both land and water. These robots used forced vibration to achieve two axis locomotion utilizing a single piezoelectric actuator.

This article describes the design, manufacture and performance of a prototype miniature hexapod robot shown in Fig. 1. The following section will detail the robot's configuration and the process by which it was designed. Subsequently the

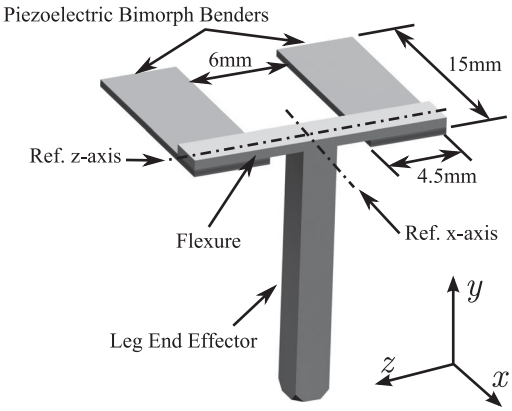

Fig. 2. MinRAR leg configuration.

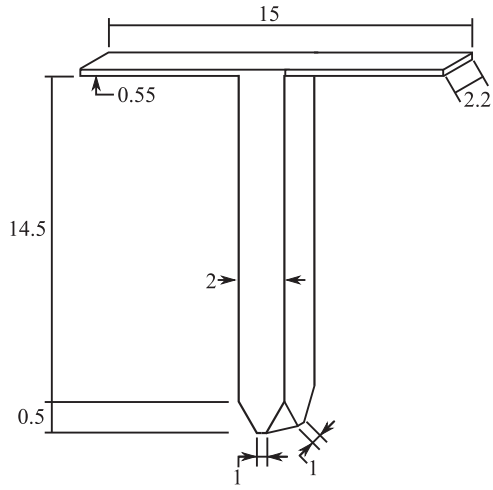

Fig. 3. Leg schematic, all dimensions in mm.

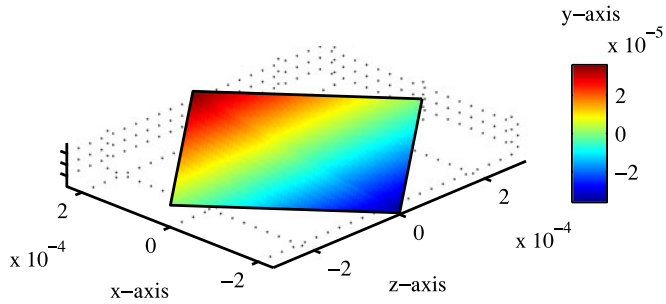

Fig. 4. Approximate operational space of the prototype leg end-effector in 3-D.

construction methodology and electrical configuration are described followed by a detailed description of the control methodology and driving signals for the robot. Lastly the experimental method is described and the article is concluded with a comparison to similar existing miniature robots.

II. Configuration

The Miniature Resonant Ambulatory Robot (MinRAR V1), shown in Fig. 1, is a six legged robot approximately 50 mm in length that utilizes piezoelectric bimorph benders to produce a walking motion. Each leg consists of two bimorph benders mounted side-by-side and joined at the tip by a flexure and end-effector. A walking motion is achieved when the two benders are driven 90° out-of-phase. This phase difference is henceforth referred to as the 'step-phase'.

The robot's leg configuration, shown in Fig. 2 was previously described in [25], where it was found that if the first and second resonance modes were made to overlap, a walking motion could be produced at resonance. This work also identified a lumped mass model that was used to design the flexure and end-effector so that the first two resonance modes were as close as possible.

III. Design & Construction

A. Leg End-Effector Design

In the interest of rapid prototyping, the leg end-effectors and body of the robot were 3-D printed using an ABS FDM printer. This technique allowed for custom shapes to be rapidly created but limited the minimum feature size to 0.5 mm. This restricts the number of parameters that can be changed to modify the resonance modes of the robot. Due to these limitations, the focus of the end-effector design was to maximize the lifting and swinging displacement for locomotion.

Dimensions of the end-effector and flexure are listed in Fig. 3. These dimensions were chosen as a reasonable starting point that would produce sufficient swing and lifting motions in the leg when driven below resonance and provide a moderately close matching of the first and second resonance modes. Fig. 4 shows the maximum available work space of the end effector; however, when driven 90° out-of-phase, the effective maximum displacements are 51 μm in the y-axis, 330 μm in the x-axis and 295 μm along the z-axis.

The lumped mass models described in [25] comprise equations that describe the effective stiffness and mass for a given degree of freedom. These have been modified slightly to account for the stiffer plastic flexure. For the x-axis rotational DoF or 'swinging' DoF, the effective rotational stiffness (J_x) and rotational inertia (I_x) is,

$$J_x = \frac{J_{\mathrm{Fx}} J_{\mathrm{Px}}}{J_{\mathrm{Fx}} + J_{\mathrm{Px}}}, I_x = I_{\mathrm{Px}} B^2 + \frac{I_L}{2} \tag{1}$$

$$B = \frac{J_{\mathrm{Fx}}}{J_{\mathrm{Fx}} + J_{\mathrm{Px}}}, \tag{2}$$

where the subscripts F, P and L refer to the flexure, bender and leg respectively.

The other DoF of interest is the rotation about the z-axis or 'lifting' DoF. The effective stiffness and inertia for this DoF is,

$$J_z = \frac{J_{\mathrm{Fz}} J_{\mathrm{Pz}}}{J_{\mathrm{Fz}} + J_{\mathrm{Pz}}}, I_z = I_{\mathrm{Pz}} C^2 + \frac{I_L}{2}, \tag{3}$$

$$C = \frac{J_{\mathrm{Fz}}}{J_{\mathrm{Fz}} + J_{\mathrm{Pz}}}. \tag{4}$$

The reason for the difference between this result and the work of [25] is that the stiffness of the flexure is closer to that of

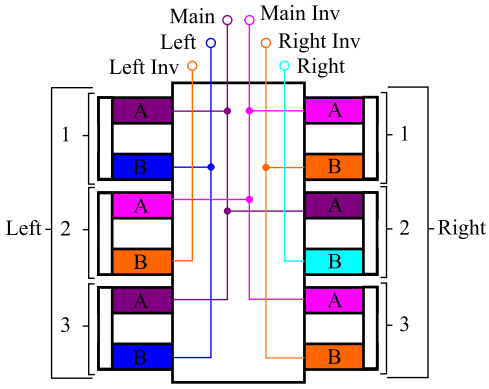

Fig. 5. Actuator wiring diagram.

the bender and therefore the bender stiffness must be taken into account. It is also important to note that the over constrained nature of the system is not accounted for in this model. Specifically, the stretching of the flexure as well as any side bending or twisting of the actuator is ignored. Additionally, S-shaped bending of the actuator can also be ignored since the added stiffness of the flexure across the tip of the actuator is minimal.

Using $f = \frac{1}{2\pi}\sqrt{\frac{J}{I}}$ and the above equations for stiffness and inertia, the resonance frequency for lifting and swinging DoFs are approximately 566 Hz and 655 Hz respectively. A finite element analysis was also performed using ANSYS which predicts the first and second resonance modes to occur at 666 Hz and 672 Hz respectively.

B. Assembly

The body of MinRAR V1 was printed in two halves to allow the piezoelectric actuators to be affixed between them using two-part epoxy. In order to improve leg lift height, the legs were mounted at an angle of 30° to make use of the high displacement along the x-axis. The leg end-effectors were glued to the tips of the actuators using a high strength epoxy glue and a specialized mount to hold the legs in place during assembly. A PCB was mounted on top of the robot to breakout the drive signals for each piezoelectric actuator as per Fig. 5.

One downside to this construction method is that approximately 3 mm of the piezoelectric bender must be embedded into the body of the robot to properly mount the actuators. In addition, the soldered wire connection on each actuator makes precise mounting difficult. As a result, the piezoelectric actuators may not be perfectly aligned to each other. Consideration has not been given to the fatigue life of the robot; however, by following manufacturing principles outlined in [26] the reliability of the robot could be improved.

C. Electrical Configuration

Control of the prototype robot is achieved using three drive signal pairs comprised of the main, left and right signals and three 180° out-of-phase complementary drive signals. Fig. 5 shows the electrical wiring diagram for the piezoelectric actuators. The three primary drive signals were generated using a National Instruments MyRio microcontroller with analog inputs to control the frequency, phase and peak-to-peak amplitude. An additional PCB was designed to create the three 180° out-of-phase auxiliary drive signals using simple op-amp inverting amplifiers.

The actuators are 15 mm × 4.5 mm × 0.4 mm PZT-5A bimorph benders supplied by Piezo Systems. These actuators were driven using the biased bipolar driving method. This method was chosen as it produces the largest possible deflection by utilizing the maximum positive and negative electric fields [27]. The piezoelectric material has a maximum permissible driving voltage of up to 200 V or down to −50 V as calculated from the maximum polling and coercive field strengths for the material. When driven with a sine wave at these voltages and off resonance, the expected power draw will be approximately 7.1 $\mathrm{mW/Hz}$ based on the PiezoDrive.com power calculator. The high voltage drive signals for these actuators were generated by two three-channel high voltage amplifiers custom built in the Precision Mechatronics Lab.

IV. Control Methodology

The ambulatory motion of the hexapod is created by driving the robot with a tripod gait [28]. In the tripod gait, legs are operated in two groups of three that are 180° out-of-phase with each other, nominally a primary and an inverted set of drive signals. The tripod gait provides a high speed statically stable walking gait with a minimal number of drive signals required. As well as the pair of tripods drive signals, a further distinction needs to be made between the left-hand and right-hand side legs so that the robot can perform turns. This results in a set of six drive signals; these are the main, left and right primary drive signals and their corresponding inverse signals as described in the previous section.

As previously mentioned, the step-phase is the phase difference between the main drive signal, and the left or right hand drive signals. The step-phase controls the proportion of lift and swing that occurs during each step cycle. For example, when the step-phase is 0°, the actuators for each leg are moving in sync and therefore the only motion that is produced is lifting. Similarly, if the step-phase is 180°, the motion of the actuators will cause the leg to produce a pure swinging motion. Nominally a 90° step-phase will produce an even combination of lifting and swinging motion which will create an ambulatory motion in the robot. Increasing the step-phase will increase the length of each step and therefore the speed of the robot; however, this will reduce the maximum leg lift height. A controller should be used to optimize the step-phase for maximum step distance and velocity based on the gross mass of the robot and the roughness of the surface.

To drive the robot in a straight line, the step-phase of the left and right hand side drive signals must be equivalent. The robot can also be made to turn left or right by reducing the step-phase of the left or right side legs while maintaining the other side. For example, for the robot to turn left, the left side legs can be driven in a pure lifting motion with a step-phase of 0° while the right side legs are driven with a standard 90° step-phase. The

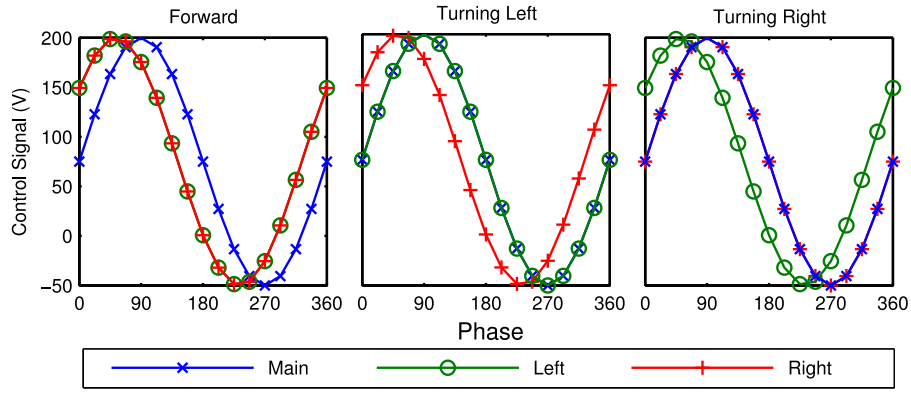

Fig. 6. Drive signal diagram.

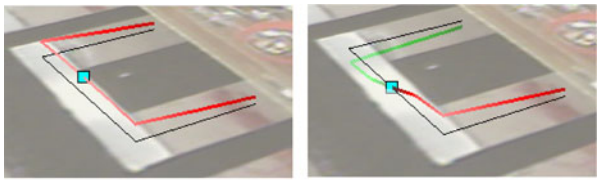

Fig. 7. Mode shapes of the first and second resonance modes.

TABLE I
MEASURED RESONANCE FREQUENCIES AND MAGNITUDE FOR EACH LEG

Leg	1st Mode		2nd Mode	
	Freq	Mag (um/V)	Freq	Mag (um/V)
Left 1	558 Hz	10.1 dB	701 Hz	9.2 dB
Left 2	677 Hz	14.8 dB	772 Hz	9.2 dB
Left 3	596 Hz	8.6 dB	715 Hz	9.3 dB
Right 1	689 Hz	13.1 dB	808 Hz	9.8 dB
Right 2	509 Hz	8.1 dB	585.9 Hz	10.1 dB
Right 3	578 Hz	9 dB	728 Hz	9.5 dB

robot can also be made to turn on the spot by reducing the step-phase below 0° such that $\phi_{\text{left}} = -\phi_{\text{right}}$, that is, the left legs are moving forward, and the right hand legs are moving backwards, or visa versa. Similarly, if the left and right hand side legs are driven with an equivalent negative step-phase, the robot will walk backwards. Fig. 6 shows the corresponding drive signals for producing forward, turning left and turning right motion.

V. PERFORMANCE

The performance of MinRAR V1 was measured by carrying out a frequency response analysis on each leg in free air. A pseudo-random noise signal was applied to one piezoelectric actuator in each leg with the other actuator open circuit. The displacement was measured using a Polytec scanning vibrometer. Fig. 7 shows the mode shapes for the first and second resonance modes. As predicted, the first mode produces a lifting motion and the second mode produces a swinging motion.

The frequency and magnitude of the first and second resonance modes for each leg are listed in Table I. The frequency response correlates reasonably well with the analytical results

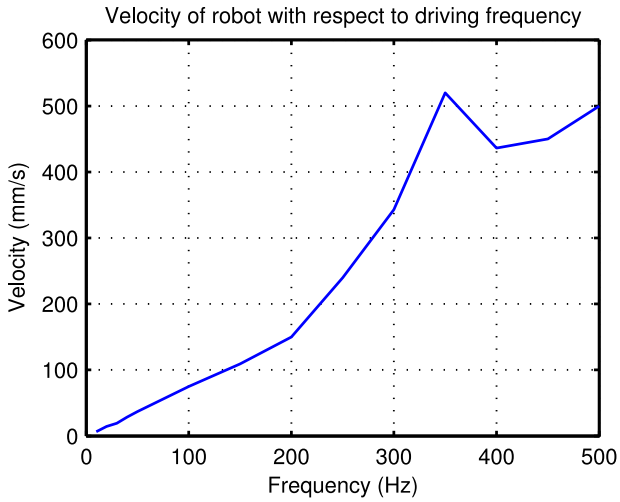

Fig. 8. Forward velocity of robot from 1 to 500 Hz with a 90° step phase.

in Section III with some legs matched more closely than others. The principle cause of variations between the legs is the imperfect mounting of the piezoelectric actuators. This creates variations in the free length, stiffness, and the separation distance between the actuator pairs. There is also some added twisting stiffness in the piezoelectric actuator that isn't taken into account in the lumped mass model that effects the rotation about the x-axis DoF. Lastly, variation in the d_{31} constant and the modulus of elasticity occur when under high electric field and strain [26]. These changes could also be the cause for the discrepancy between the predicted and measured resonances.

A. Low Frequency Operation

The low frequency operation was characterized by driving the robot over a distance of 30 cm on a hard flat surface with a sprayed rubber coating. The robot was filmed at 50 fps using a DSLR camera. The frequency was increased in 10 Hz increments, starting at 1 Hz up to 50 Hz, then in 50 Hz increments up to 500 Hz and plotted in Fig. 8. The response is mostly linear, however a peak in the curve is observed at approximately 350 Hz. By driving the robot at this frequency the legs are able to achieve larger displacements and therefore the robot was able to travel faster.

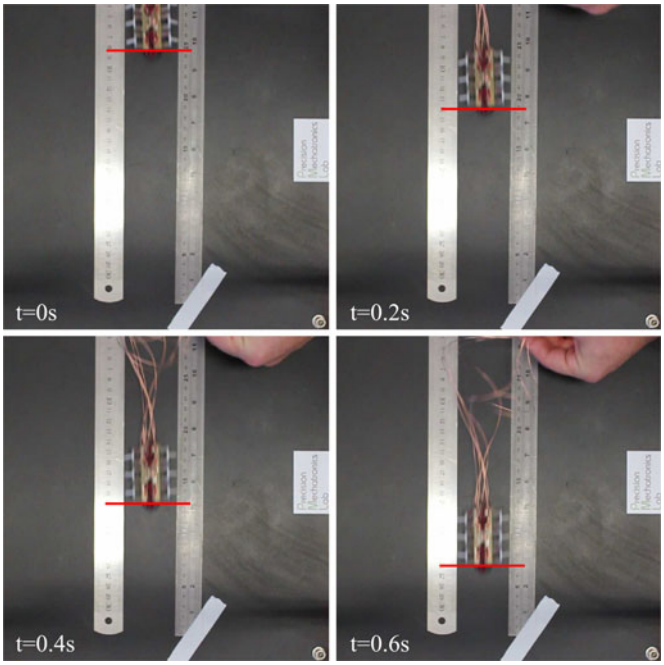

Fig. 9. MinRAR being driven at 250 Hz with a step phase of 90° and 0.2 seconds between each frame.

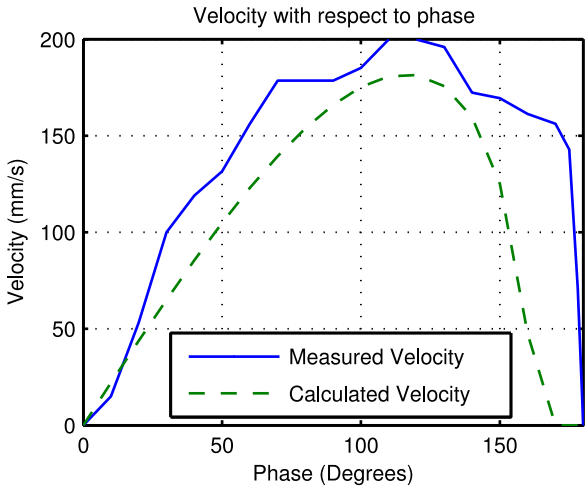

Fig. 10. Forward velocity of robot when driven at 250 Hz with a step-phase of 0° to 180°.

When the robot was driven with frequencies above 300 Hz, some observable loss of traction occurred during start-up. This slipping effect can be mitigated by increasing the coefficient of friction by coating the tip in a rubberized paint or by controlling the acceleration of the robot from a static position. Fig. 9 shows the velocity-frequency test that was performed on MinRAR V1 at 250 Hz driving frequency, with 0.2s intervals between still frames and a step phase of 90°.

The relationship between step-phase and velocity was also explored. A test was performed by driving the robot at a frequency of 250 Hz and increasing the step-phase in 10° increments from 0° to 180°. Fig. 10 shows the measured and predicted velocity. The calculated velocity was found from,

$$v = 2d_{\text{swing}}\left(1 - \frac{d_{\text{lift,gnd}}}{d_{\text{lift,max}}}\right) f, \tag{5}$$

where d_{swing} is the maximum leg swing distance of each leg for a given phase, $d_{\text{lift,gnd}}$ is the lift height required to achieve ground clearance, $d_{\text{lift,max}}$ is the maximum leg lift height for a given phase and f is the frequency. If $d_{\text{lift,gnd}} > d_{\text{lift,max}}$ then $v = 0$.

The experimental and analytical results for velocity compared to frequency align reasonably well. The curves show a peak in the velocity at approximately 110°. The primary reason for the differences between the two curves is a stick-sip effect [29] between the end effector and the ground. This effect causes forward motion to occur while both feet are still touching the ground. An additional source of discrepancy is the variations in actuator mounting and free length.

There are two properties that strongly affect the velocity-phase relationship, the minimum leg lift height ($d_{\text{lift,gnd}}$) for ground clearance, and the frictional properties of the leg/ground interface. $d_{\text{lift,gnd}}$ is primarily affected by the mass of the robot and the stiffness of the legs such that $d_{\text{lift,gnd}} = \frac{W}{3K_y}$, where W is the weight of the robot. Put simply, as the robot becomes more loaded the legs need to apply more force to overcome the deflection due to the mass of the robot and the longer both legs are simultaneously touching the ground for, the less time the legs are free to produce forward locomotion.

While the mass of the robot is somewhat controllable, the coefficient of friction at the ground and end effector interface is unknown. The strength of the frictional forces will effect the stick-slip response that occurs during the cross-over period between striding and swinging when all 6 legs are concurrently touching the ground. As the step-phase increases, the leg lift height decreases and the stick-slip effect becomes more pronounced. Variation in the results shown in Figs. 10 and 8 are attributed to degradation in the PZT material from repeated usage.

B. Resonant Locomotion

A mount was designed for the robot that restricted the movement of the robot in the xz-plane while allowing for free movement in the y-axis. This arrangement will simulate the effects of ground contact on the frequency response. The robot was driven using a tripod gait and the frequency was swept from 1 to 1000 Hz in 1 Hz frequency steps with 10 cycles applied at each frequency step. The driving voltage was limited to 10 % of the maximum driving voltage (25 V peak-to-peak) to protect the robot from any stray resonance modes while allowing enough deflection to achieve minimal ground clearance. The velocity was measured at the center point of the flexure using a Polytec vibrometer and the time varying data integrated to generate a plot of displacement vs frequency. The frequency response was also measured in free air, both of which are shown in Fig. 11.

The free air response of the robot features two large resonance modes close to 700 Hz and 800 Hz at approximately 12 dB and 6 dB respectively. The frequency response for the ground contact

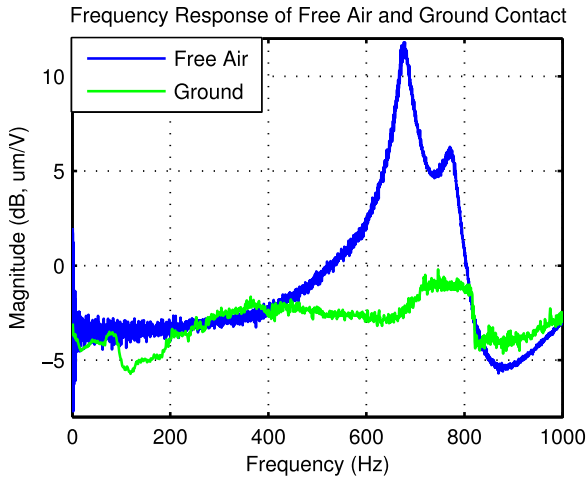

Fig. 11. A frequency response comparison of the leg in free-air and ground contact.

TABLE II
PERFORMANCE OF MINIATURE ROBOTS

Robot	Mass	Length	Speed	Tethered?
HAMR 3	1.7 g	48 mm	42 mm/s	No
Soft Robot [16]	80 g	182 mm	4 mm/s	Yes
m-DoF [18]	2.1mg/leg	–	27 mm/s	Yes
Hariri 1 [23]	3.25 g	50 mm	40 mm/s	Yes
LPMR [22]	6.27 g	50 mm	246.5 mm/s	No
MinRAR V1	16 g	55 mm	520 mm/s	Yes

shows a significantly flatter response with a slight amplification at 350 Hz and a more significant peak between 750 to 800 Hz. Driving this robot at the higher resonance frequency is not recommended due to the possibility of destructive amplification of the piezoelectric actuators if a loss in ground contact occurs,such as when walking over a crack or bump in the ground.

The flatness of the response allows the robot to be driven over a broad frequency range with a relatively linear response. The robot can be driven at a frequency of 350 Hz for a small gain in the forward velocity. By driving the robot at this resonance there is no risk of damage to the actuators. When compared to the free air response, the ground contact effect is similar to an increase in damping which is related to the total mass of the robot.

C. Performance Comparison

Although this robot is only a prototype designed to test the mode of locomotion and construction method, it performs reasonably well when compared to similar robots. Table II compares the speed, mass and abilities of several other robots with the MinRAR V1 robot. The MinRAR V1 outperformed other robots in terms of raw speed, but tended to be heavier and lacked on-board electronics.

VI. CONCLUSION

A miniature resonant ambulatory robot (MinRAR V1) was presented which utilizes bimorph piezoelectric actuators to produce an ambulatory motion. The focus of this work was to test the proposed driving methodology and leg configuration on a fully realized miniature robot by applying the previously described 3D lumped mass model in the design of the flexure and end-effector [25]. The robot was able to achieve forward locomotion speeds of up to 520 mm/s or approximately 10 body lengths per second with a driving frequency of 350 Hz and a step-phase of 90°.

The effect of varying the ratio of leg lift to leg stride distance was also investigated. An experiment was performed that identified an optimal step-phase of approximately 110° when driven on a smooth and high friction surface. When the friction of the driving surface was altered, a significant loss of traction was observed during high speed start up. Lastly, the predicted locomotion speed was found to be higher than expected due to a stick-slip effect that was occurring during the transition from lifting to swinging of the legs.

The experimental work highlighted the importance of a uniform mechanical construction for attaining consistent resonance modes across all legs. This can be improved by simplifying the manufacturing process and reducing the assembly steps. Another approach is to fine tune the resonance modes after construction by adding small lumped masses to the tips of the end-effector or ends of the actuator.

Lastly, a frequency response analysis was performed to determine the effect of ground contact on the resonance modes of the robot. This test showed the ground contact to produce a significant damping like effect of the resonance modes, but highlighted a small resonance mode at approximately 350 Hz.

Future work will involve the implementation of control strategies to maintain optimal step-phase and frequency with an aim to achieve a desired forward velocity. The power supply and control electronics will also be miniaturized to allow for autonomous, un-tethered operation. Finally, the manufacturing process will be streamlined to improve the uniformity of the piezoelectric actuators and the resonance response of the legs.

REFERENCES

[1] C. Zhu, "In-pipe robot for inspection and sampling tasks," *Ind. Robot Int. J.*, vol. 34, no. 1, pp. 39–45, 2007.
[2] J. Casper and R. R. Murphy, "Human-robot interactions during the robot-assisted urban search and rescue response at the World Trade Center," *IEEE Trans. Syst., Man, Cybern. Part B, Cybern.*, vol. 33, no. 3, pp. 367–85, Jan. 2003.
[3] L. Zhang, Q. Huang, Y. Li, J. Gao, H. Li, and L. Wu, "Research and development of throwable miniature reconnaissance robot," in *Proc. 2012 IEEE Int. Conf. Mechatronics Autom.*, Aug. 2012, pp. 1254–1259.
[4] T. Seo and M. Sitti, "Tank-like module-based climbing robot using passive compliant joints," *IEEE/ASME Trans. Mechatronics*, vol. 18, no. 1, pp. 397–408, Feb. 2013.
[5] O. Dolghi, K. W. Strabala, T. D. Wortman, M. R. Goede, S. M. Farritor, and D. Oleynikov, "Miniature in vivo robot for laparoendoscopic single-site surgery," *Surgical Endoscopy*, vol. 25, no. 10, pp. 3453–3458, Oct. 2011.
[6] J. Huang, S. M. Farritor, A. Qadi, and S. Goddard, "Localization and follow-the-leader control of a heterogeneous group of mobile robots," *IEEE/ASME Trans. Mechatronics*, vol. 11, no. 2, pp. 205–215, Apr. 2006.
[7] J. A. Paradiso and T. Starner, "Energy scavenging for mobile and wireless electronics," *IEEE Pervasive Comput.*, vol. 4, no. 1, pp. 18–27, Jan. 2005.
[8] S. Miyashita, S. Guitron, M. Ludersdorfer, C. R. Sung, and D. Rus, "An untethered miniature origami robot that self-folds, walks, swims, and degrades," in *Proc. 2015 IEEE Int. Conf. Robot. Autom.*, 2015, pp. 1490–1496.

[9] D. Chen, J. Yin, K. Zhao, W. Zheng, and T. Wang, "Bionic mechanism and kinematics analysis of hopping robot inspired by locust jumping," *J. Bionic Eng.*, vol. 8, no. 4, pp. 429–439, 2011.
[10] R. Sahai, S. Avadhanula, R. Groff, E. Steltz, R. Wood, and R. S. Fearing, "Towards a 3g crawling robot through the integration of microrobot technologies," in *Proc. 2006 IEEE Int. Conf. Robot. Autom.*, 2006, pp. 296–302.
[11] M. Kovac, M. Bendana, R. Krishnan, J. Burton, M. Smith, and R. J. Wood, "Multi-stage micro rockets for robotic insects," in *Robot.: Science and System VIII*. Cambridge, MA, USA: MIT Press, 2013, Art. no. 185.
[12] A. T. Baisch, P. S. Sreetharan, and R. J. Wood, "Biologically-inspired locomotion of a 2g hexapod robot," *Int. Conf. Intell. Robots Syst.*, 2010, pp. 5360–5365.
[13] J. P. Whitney and R. J. Wood, "Conceptual design of flapping-wing micro air vehicles," *Bioinspiration Biomimetics*, vol. 7, no. 3, Sep. 2012, Art. no. 036001.
[14] K. Y. Ma, P. Chirarattananon, S. B. Fuller, and R. J. Wood, "Controlled flight of a biologically inspired, insect-scale robot," *Science*, vol. 340, no. 6132, pp. 603–607, May 2013.
[15] A. T. Baisch, C. Heimlich, M. Karpelson, and R. J. Wood, "HAMR3: An autonomous 1.7g ambulatory robot," in *Proc. 2011 IEEE/RSJ Int. Conf. Intell. Robots Syst.*, 2011, pp. 5073–5079.
[16] C. T. Nguyen *et al.*, "Printable monolithic hexapod robot driven by soft actuator," in *Proc. 2015 IEEE Int. Conf. Robot. Autom.*, 2015, pp. 4484–4489.
[17] B. Edamana and K. R. Oldham, "Optimal low-power piezoelectric actuator control with charge recovery for a microrobotic leg," *IEEE/ASME Trans. Mechatronics*, vol. 18, no. 1, pp. 251–262, Feb. 2013.
[18] C.-H. Rhee, J. S. Pulskamp, R. G. Polcawich, and K. R. Oldham, "Multi-degree-of-freedom thin-film PZT-actuated microrobotic leg," *J. Microelectromechanical Syst.*, vol. 21, no. 6, pp. 1492–1503, 2012.
[19] J. H. Ryou and K. R. Oldham, "Dynamic characterization of contact interactions of micro-robotic leg structures," *Smart Mater. Struct.*, vol. 23, no. 5, 2014, Art. no. 55014.
[20] H. Hariri, Y. Bernard, and A. Razek, "A traveling wave piezoelectric beam robot," *Smart Mater. Struct.*, vol. 23, no. 2, 2013, Art. no. 25013.
[21] H. Hariri, Y. Bernard, and A. Razek, "Dual piezoelectric beam robot: The effect of piezoelectric patches positions," *J. Intell. Mater. Syst. Struct.*, vol. 26, no. 18, pp. 2577–2590, 2015.
[22] H. H. Hariri, L. A. Prasetya, G. S. Soh, S. Foong, K. Otto, and K. Wood, "A tether-less legged piezoelectric miniature robot using bounding gait locomotion for bidirectional motion," *Proc. 2016 IEEE Int. Conf. Robot. Autom.*, 2016, pp. 4743–4749.
[23] H. H. Hariri, G. S. Soh, S. H. Foong, K. L. Wood, and K. Otto, "Miniature piezoelectric mobile robot driven by standing wave," in *Proc. 14th Int. Fed. Promotion Mech. Mach. Sci. World Congr.*, 2015, pp. 325–330.
[24] F. Becker, "Piezo-driven micro robots for different environments: Prototypes and experiments," in *Proc. 7th German Conf. Robotik*, 2012, pp. 41–45. [Online]. Available: http://ieeexplore.ieee.org/xpls/abs_all.jsp?arnumber=6309478
[25] S. A. Rios, A. J. Fleming, and Y. K. Yong, "Design of a two degree of freedom resonant miniature robotic leg," in *Proc. 2015 IEEE IntAdv. Intell. Mechatronics. Conf.*, Jul. 2015, pp. 318–323.
[26] N. T. Jafferis, M. J. Smith, and R. J. Wood, "Design and manufacturing rules for maximizing the performance of polycrystalline piezoelectric bending actuators," *Smart Mater. Struct.*, vol. 24, no. 6, 2015, Art. no. 65023.
[27] S. A. Rios and A. J. Fleming, "A new electrical configuration for improving the range of piezoelectric bimorph benders," *Sensors Actuators A, Phys.*, vol. 224, pp. 106–110, 2015.
[28] K. S. Espenschied, H. J. Chiel, R. D. Quinn, and R. D. Beer, "Leg coordination mechanisms in the stick insect applied to hexapod robot locomotion," *Adaptive Behavior*, vol. 1, no. 4, pp. 455–468, 1993.
[29] R. P. Nachane, G. F. S. Hussain, and K. R. K. Iyer, "Theory of stick-slip effect in friction," *Indian J. Fibre Textile Res.*, vol. 23, no. 4, pp. 201–208, 1998.